is no inherent gain in stability, at least as measured by ΔH, on forming the bimetallic complex. The absence of any monostannacarborane–bipyrimidine is most likely due to the preparative procedure. The complexes were purified by sublimation, and it is likely that any monostannacarborane product formed would decompose during sublimation to give the less volatile bimetallic compound. It should be noted that the NMR spectral or spectroscopic data reported in the Experimental Section were obtained on solutions of the purified bimetallic complex dissolved in C_6D_6.

The trans orientation of the stannacarboranes in VII seems to be dictated on steric grounds. Table V lists some calculated optimized parameters for the cis isomer of the model compound. Calculations show that there is very little energy difference between the two isomers (≈2 kcal/mol). The cis isomer has slightly longer Sn–N bonds, an increased slippage of the Sn, and a larger dihedral angle than the trans isomer. Although the differences are small, they are consistent with a higher repulsion between the stannacarborane units in the cis isomer. The individual atomic interactions can be analyzed by partitioning the total energy of the molecules into a series of one- and two-center energy terms.[24,25] Such a partitioning was found to be useful in explaining the geometry of the $(C_{10}H_8N_2)SnC_2B_4H_6$ complex.[22] A comparison of the two center terms in the cis and trans complexes shows that an increase in repulsion between the unique borons of the carboranes is found in going from the trans to the cis isomer (see Table V for interatomic distances). The small energy difference between the two isomers indicates that there should be an easy conversion between the two forms. Indeed, the solution spectral data presented (see Experimental Section) for compounds VII, VIII, and IX could be that of a mixture of the two isomers. From the differences in dipole moments shown in Table V, it may be possible to isolate the cis complex by recrystallization from a polar solvent.

Acknowledgment. This work was supported by grants from the National Science Foundation (CHE-8800328), the Robert A. Welch Foundation (N-1016), and the donors of the Petroleum Research Fund, administered by the American Chemical Society. We thank Dr. Charles Campana (Nicolet Instruments Corp.) and Professor Larry Dahl (University of Wisconsin at Madison) for their help in obtaining the crystal structure of VII.

Registry No. I, 90388-43-5; II, 91670-63-2; III, 91686-40-7; IV, 120829-86-9; V, 120829-83-6; VI, 120829-84-7; VII, 110374-95-3; VIII, 120853-36-3; IX, 120829-85-8.

Supplementary Material Available: Listings of mass spectrometric data (Table S-I) and IR absorptions (Table S-II) of IV, V, VI, VII, VIII, and IX, tables of anisotropic displacement coefficients of IV (Table S-III) and VII (Table S-VII), additional tables of bond lengths, bond angles, and torsion angles for IV (Table S-IV) and VII (Table S-VIII), tables of H-atom coordinates and isotropic displacement coefficients for IV (Table S-V) and VII (Table S-X), and a table of deviations of the atoms from the plane formed by C_2B_3 and bipyrimidine ring (Table S-IX) for VII (24 pages); listings of structure factors of IV (Table S-VI) and VII (Table S-IX) (40 pages). Ordering information is given on any current masthead page.

(24) Dewar, M. J. S.; Lo, D. H. J. Am. Chem. Soc. **1971**, *93*, 7201.
(25) Olivella, S.; Vilarrusa, J. *J. Heterocycl. Chem.* **1981**, *18*, 1189.

UV Photoelectron Spectra and Electronic Structure of 1,2-Diosmacyclopropane and 1,2-Diosmacyclobutane Complexes

Bruce R. Bender,[1a] Renzo Bertoncello,[1b] Michael R. Burke,[1d] Maurizio Casarin,[1c] Gaetano Granozzi,*[1b] Jack R. Norton,*[1a] and Josef Takats*[1d]

Department of Chemistry, Colorado State University, Fort Collins, Colorado 80523, Dipartimento di Chimica Inorganica, Metallorganica ed Analitica, Università di Padova, via Loredan 4, 35131 Padova, Italy, Istituto di Chimica e Tecnologia dei Radioelementi del CNR, Padova, Italy, and Department of Chemistry, University of Alberta, Edmonton, Alberta, Canada, T6G 2G2

Received February 22, 1989

The electronic structures of two isolobal analogues of cyclopropane and cyclobutane, $Os_2(CO)_8(\mu\text{-}CH_2)$ and $Os_2(CO)_8(\mu\text{-}C_2H_4)$, have been investigated by means of gas-phase UV photoelectron (PE) spectroscopy and DV–Xα MO calculations. A comparison between the bonding schemes of the organic and organometallic partners reveals that the qualitative features of the bonding in these molecules are in accord with the concept of the isolobal analogy. However, differences are found when a quantitative description of the bonding is attempted since the metal complexes contain an additional framework MO with significant Os–C antibonding character. This feature is due to the involvement of the t_{2g}-like MOs of the metallic fragments with the interactions within the dimetallacycle. The UV–PE data lend support to the picture arising from the theoretical calculations.

Introduction

In recent years Hoffmann[2] has elegantly and exhaustively demonstrated the value of comparing the frontier orbitals of various metal–ligand combinations with those of hydrocarbon fragments (CH_3, CH_2, and CH). Stone[3] has also very successfully used this "isolobal connection" to guide the preparative work on, and to rationalize the structures of, complexes containing metal–metal bonds. The triangulo $M_3(CO)_{12}$ clusters (M = Ru, Os) can be

(1) (a) Colorado State University. (b) University of Padova. (c) CNR of Padova. (d) University of Alberta.
(2) Hoffmann, R. *Angew. Chem., Int. Ed. Engl.* **1982**, *21*, 711.
(3) Stone, F. G. A. *Angew. Chem., Int. Ed. Engl.* **1984**, *23*, 89.

0276-7333/89/2308-1777$01.50/0

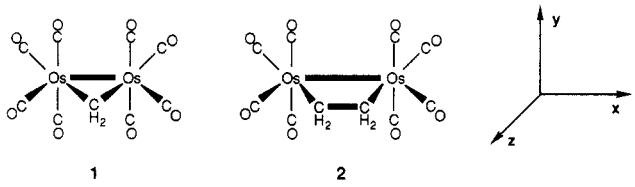

1 2

Figure 1. Schematic drawing of $Os_2(CO)_8(\mu\text{-}CH_2)$ (1) and $Os_2(CO)_8(\mu\text{-}C_2H_4)$ (2). The adopted axis system is also shown.

regarded as isolobal analogues of cyclopropane (CH_2 is isolobal with the d^8 $M(CO)_4$ fragment), and this suggestion has been of value for the analysis of the electronic structures of these complicated molecules.[4] Following similar arguments, the complexes $M_2(CO)_8(\mu\text{-}CH_2)$ are analogues of cyclopropane, while $M_2(CO)_8(\mu\text{-}C_2H_4)$ and $M_4(CO)_{16}$ are analogues of cyclobutane. Recently examples of all three situations have been described when the metal is osmium.[5,6] Interestingly, the loss of ethylene from the 1,2-diosmacyclobutane $Os_2(CO)_8(\mu\text{-}\eta^1,\eta^1\text{-}C_2H_4)$ is reversible and stereospecific,[7] suggesting that, contrary to the predictions of traditional orbital symmetry arguments applied to cyclobutane,[8] this fragmentation is concerted. Furthermore, the loss of ethylene is facile and provides a versatile synthetic strategy for the preparation of a variety of related 1,2-diosmacycles.[9]

In view of the current interest in dimetallacycles, an accurate analysis of the metal–metal and metal–ligand multicentered interactions in such complexes is of obvious value. In addition to providing information that could contribute to a better understanding of the nature of metal–olefin interactions on metal surfaces,[10] such studies are needed to delineate the limits at which the detailed electronic structures of isolobal analogues can be realistically compared.

Some of us have recently demonstrated that gas-phase UV photoelectron (PE) spectroscopy can provide a detailed description of the electronic structure of polynuclear organometallic molecules,[4a,b,11] particularly when coupled with quantum mechanical calculations. Actually, the PE technique maps the energy of the outermost occupied molecular orbitals (MOs) and thus provides an experimental test for the results of the theoretical calculations which, on their own, furnish informations concerning the bonding scheme.

We report here a study of the isolobal analogues of cyclopropane and cyclobutane, $Os_2(CO)_8(\mu\text{-}CH_2)$ (1) and $Os_2(CO)_8(\mu\text{-}C_2H_4)$ (2) (see Figure 1), carried out by using UV–PE spectroscopy and nonrelativistic DV–Xα calculations.

Experimental Section

Samples for PE measurements were obtained by published procedures[5] (2 was obtained via the photochemical route) and their purity was checked by IR and NMR spectroscopy. $Os_2(CO)_8(\mu\text{-}^{13}C_2H_4)$, 2-$^{13}C_2$, was prepared from labeled ethylene (Cambridge Isotope Laboratories, 99% $^{13}C_2$) and $Os_3(CO)_{12}$ by the same procedure. Its 200-MHz NMR spectrum was obtained in CD_2Cl_2 on an IBM-Bruker WP-200 spectrometer. ^1J(C–C) was determined by matching the experimental spectrum with spectra simulated for various values of the coupling constant. The spectra were simulated by using PANIC, a version of LAOCOON III adapted for use on an Aspect 2000 minicomputer.

He I (21.217 eV) and He II (40.814 eV) excited PE spectra were recorded on a Perkin-Elmer PS-18 spectrometer modified by inclusion of a hollow-cathode discharge lamp giving high output of He II photons. The ionization energy (IE) scale was calibrated by reference to admitted inert gases (Xe–Ar) and to the He $1s^{-1}$ self-ionization. A heated inlet probe system was used at 40 °C. No evidence of sample decomposition was observed during the recording of the spectra.

Calculations. Hartree–Fock–Slater (HFS) discrete variational (DV–Xα) calculations[11] were performed on a VAX 8600 computer (DEC).

The approximations in the reported theoretical calculations are (i) use of near-minimal AO basis sets, (ii) a least-squares fit of the model electron density to the true density according to the procedure reported in ref 13, (iii) use of the Gaspar–Kohn–Sham exchange potential,[14] and (iv) neglect of relativistic effects. The last approximation may be particularly severe when dealing with third-series transition metals. For this reason the results of the calculations reported here must be considered semiquantitative, and we shall be interested in comparisons between the bonding schemes and the one-electron energy levels of the molecules studied rather than in absolute energy values. An estimate of the magnitude of electronic relaxation upon ionization has been obtained by carrying out calculations using the Slater's transition state (TS) formalism.[15]

Numerical atomic orbitals (through 6p on Os, 2p on C, O, and 1s on H) obtained for the neutral atoms were used as basis functions. Due to the size of the systems investigated, orbitals 1s–5p (Os) and 1s on both carbon and oxygen were treated as a part of a frozen core in the molecular calculations. Atomic orbital and bond overlap populations (OPs) were computed by using Mulliken's scheme.[16] Bond lengths and angles of 2 were taken from the X-ray structural data,[5] but assuming a planar Os_2C_2 ring (C_{2v} symmetry) and rotating the $Os(CO)_4$ moiety by 8° about the y axis toward the bridging organic ligand to take into account the observed angular distortions of the CO groups in the XZ plane. The relevant distances and angles are Os–Os = 2.884 Å, Os–C_{ring} = 2.215 Å, Os–Os–C_{ring} = 70.5°, and Os–C_{ring}–C_{ring} = 105.4°. Due to the lack of a structural determination, the geometrical parameters of 1 were estimated from those of 2 and of a relative of 1, $(\mu\text{-}H)_2Os_3(CO)_{10}(\mu\text{-}CH)_2$.[17] The Os–$C_{ring}$ distance in 1 was

(4) (a) Granozzi, G.; Tondello, E.; Bertoncello, R.; Aime, S.; Osella, D. *Inorg. Chem.* **1983**, *22*, 744. (b) Ajò, D.; Granozzi, G.; Tondello, E.; Fragalà, I. *Inorg. Chim. Acta* **1979**, *37*, 191. (c) Green, J. C.; Mingos, D. M. P.; Seddon, E. A. *Inorg. Chem.* **1981**, *20*, 2595. (d) Delley, B.; Manning, M. C.; Ellis, D. E.; Berkowitz, J.; Trogler, W. C. *Inorg. Chem.* **1982**, *21*, 2247.

(5) (a) Motyl, K. M.; Norton, J. R.; Schauer, C. K.; Anderson, O. P. *J. Am. Chem. Soc.* **1982**, *104*, 7325. (b) Burke, M. R.; Takats, J.; Grevels, F.-W.; Reuvers, J. G. A. *J. Am. Chem. Soc.* **1983**, *105*, 4092.

(6) Johnston, V. J.; Einstein, F. W. B.; Pomeroy, R. K. *J. Am. Chem. Soc.* **1987**, *109*, 8111.

(7) Hembre, R. T.; Scott, C. P.; Norton, J. R. *J. Am. Chem. Soc.* **1987**, *109*, 3468.

(8) Woodward, R. B.; Hoffmann, R. *The Conservation of Orbital Symmetry*; Verlag Chemie: Weinheim/Bergstr., 1971.

(9) (a) Takats, J. *Polyhedron* **1988**, *7*, 931. (b) Seils, F.; Takats, J.; unpublished results.

(10) For a general paper on the "cluster-surface analogy" see: Muetterties, E. L.; Rhodin, T. N.; Band, E.; Brucker, C. F.; Pretzer, W. R. *Chem. Rev.* **1979**, *79*, 91.

(11) (a) Granozzi, G.; Tondello, E.; Ajò, D.; Casarin, M.; Aime, S.; Osella, D. *Inorg. Chem.* **1982**, *21*, 1081. (b) Granozzi, G.; Benoni, R.; Tondello, E.; Casarin, M.; Aime, S.; Osella, D. *Inorg. Chem.* **1983**, *22*, 3899. (c) Granozzi, G.; Tondello, E.; Casarin, M.; Aime, S.; Osella, D. *Organometallics* **1983**, *2*, 430. (d) Granozzi, G.; Benoni, R.; Acampora, M.; Aime, S.; Osella, D. *Inorg. Chim. Acta* **1984**, *84*, 95. (e) Granozzi, G.; Tondello, E.; Bertoncello, R.; Aime, S.; Osella, D. *Inorg. Chem.* **1985**, *24*, 570. (f) Casarin, M.; Ajò, D.; Granozzi, G.; Tondello, E.; Aime, S. *Inorg. Chem.* **1985**, *24*, 1241. (g) Casarin, M.; Ajò, D.; Vittadini, A.; Granozzi, G.; Bertoncello, R.; Osella, D. *Inorg. Chem.* **1986**, *25*, 511. (h) Aime, S.; Bertoncello, R.; Busetti, V.; Gobetto, R.; Granozzi, G.; Osella, D. *Inorg. Chem.* **1986**, *25*, 4004. (i) Casarin, M.; Ajò, D.; Lentz, D.; Bertoncello, R.; Granozzi, G. *Inorg. Chem.* **1987**, *26*, 465. (j) Pilloni, G.; Zecchin, S.; Casarin, M.; Granozzi, G. *Organometallics* **1987**, *6*, 597.

(12) Averill, F. W.; Ellis, D. E. *J. Chem. Phys.* **1973**, *59*, 6412.

(13) Holland, G. F.; Manning, M. C.; Ellis, D. E.; Trogler, W. C. *J. Am. Chem. Soc.* **1983**, *105*, 2308 and references therein.

(14) (a) Gaspar, R. *Acta Phys. Acad. Sci. Hung.* **1954**, *3*, 263. (b) Kohn, W.; Sham, L. J. *Phys. Rev.* **1965**, *140*, A1133.

(15) Slater, J. C. *Quantum Theory of Molecules and Solids. The Self-Consistent Field for Molecules and Solids*; McGraw-Hill: New York, 1974; Vol. 4.

(16) Mulliken, R. S. *J. Chem. Phys.* **1955**, *23*, 1833.

(17) Shultz, A. J.; Williams, J. M.; Calvert, R. B.; Shapley, J. R.; Stucky, G. D. *Inorg. Chem.* **1979**, *18*, 319.

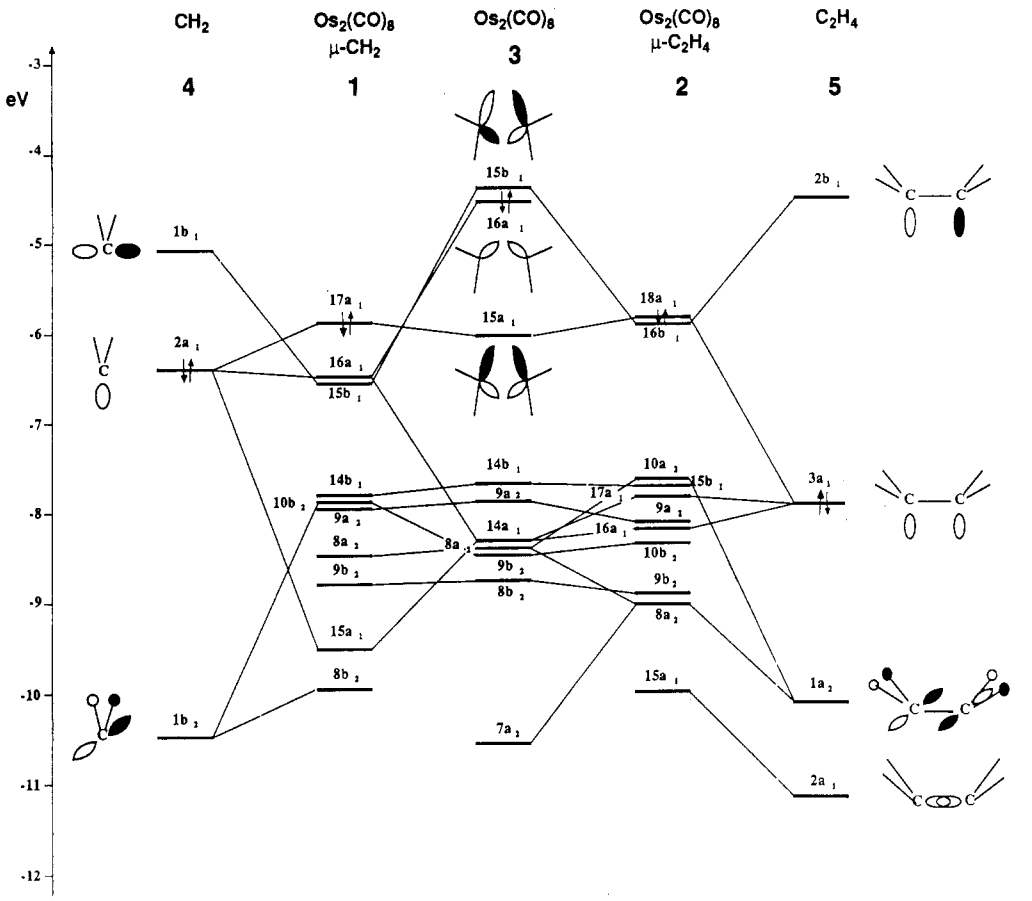

Figure 2. DV-Xα one-electron energy level diagram of $Os_2(CO)_8(\mu\text{-}CH_2)$ (1) and $Os_2(CO)_8(\mu\text{-}C_2H_4)$ (2) (planar form) starting from the levels of the constituent fragments.

set equal to that in the latter complex. However, the geometry of the $Os_2(CO_8)$ fragment in 1, including the length of the Os–Os bond, was maintained as in 2 because in the triosmium compound the Os–Os bond is supported by both a bridging methylene and bridging hydride moieties. Therefore the relevant distances and angles used in the calculations on 1 are Os–Os = 2.88 Å, Os–C_{ring} = 2.15 Å, Os–Os–C_{ring} = 48°, and Os–C_{ring}–Os = 84°.

Results and Discussion

Theoretical Results. In order to simplify the description of the bonding scheme of compounds 1 and 2, it is very useful to present a preliminary discussion of the electronic structure of the constituent fragments, namely, $Os_2(CO)_8$ (3) and the two organic moieties μ-(CH_2) (4) and μ-(C_2H_4) (5). In the solid state the four-membered Os_2C_2 ring of 2 exhibits a nonplanar puckered conformation, of C_2 symmetry.[5] In this conformation the four protons form an AA'BB' spin system. However, only a single peak has been observed in the ^1H NMR of 2 down to −90 °C. The Os_2C_2 ring is thus flexible, with a planar conformation accessible even at low temperatures. We will first discuss the results of a calculation carried out by assuming a planar Os_2C_2 ring (C_{2v} symmetry), and subsequently the implications of ring puckering will be briefly mentioned.

The frontier orbitals of a d^8 $M(CO)_4$ fragment have been extensively discussed on the basis of EHT calculations.[18,19] They can be related to those of the octahedral $M(CO)_6$ parent complex. According to preliminary calculations on the $Os(CO)_4$ fragment with the same geometry as in 2, a set of three inner orbitals, mainly d_{xy}, d_{xz}, and d_{yz} according to the axis system of Figure 1, are descended from the octahedral t_{2g} set; two outer hybrid orbitals, the first being $d_{x^2-z^2}$ with some admixture of d_{xz} and the second a mixture of s, p_x, p_z, and d_{y^2}, are related to the octahedral e_g set. The t_{2g}-like orbitals have predominantly d-to-π^*(CO) back-bonding character, while the e_g-like orbitals are mainly M–CO σ antibonding. The percentage contribution from the carbonyl ligands is higher in the e_g-like set than in the t_{2g}-like MOs.

When two $M(CO)_4$ fragments interact to give 3, Os–Os bonding and antibonding MOs are formed according to the diagram shown in Figure 2.[20] The t_{2g}-like and e_g-like sets are still distinct in 3. Within the former, both Os–Os bonding [$8b_2(\pi_{out})$, $9b_2(\delta_{out})$, $14a_1(\pi_{in})$] and Os–Os antibonding [$8a_2(\delta^*_{out})$, $9a_2(\pi^*_{out})$, $14b_1(\pi^*_{in})$] partners are occupied (in and out subscripts refer to the XZ plane). The $15a_1$ MO originates from the e_g-like dangling lobes, pointing toward the incoming bridging organic fragment, and it has a σ/π Os–Os bonding character (see Figure 2). Its antibonding counterpart is represented by the $15b_1$ LUMO. The $16a_1$ HOMO also has σ/π Os–Os bonding character, but it is characterized by substantial participation from 6s,6p metal orbitals.

The frontier orbitals of the fragments 4 and 5 are also reported in Figure 2. The $2a_1$ HOMO of 4 represents a carbon p_z donor orbital pointing toward the center of the final Os_2C ring, whereas the $1b_1$ LUMO is a carbon p_x acceptor orbital. The corresponding orbitals of 5 can be designated as $n^+(3a_1$ HOMO) and $n^-(2b_1$ LUMO) since, to a first approximation, they can be described as in-phase

(18) Elian, M.; Hoffmann, R. *Inorg. Chem.* **1975**, *14*, 1058.
(19) Burdett, J. K. *J. Chem. Soc., Faraday Trans. 2* **1974**, *70*, 1599.

(20) Interestingly, the HOMO–LUMO energy gap of $Os_2(CO)_8$, in the geometry found in 2, is computed to be very small (0.178 eV) so that some questions can be raised as to the singlet or triplet nature of its ground state.

Table I. DV-Xα Theoretical Results of $Os_2(CO)_8(\mu\text{-}CH_2)$ (1) (C_{2v})

MO	$-\epsilon$, eV	TSIE, eV	pop., % 2 Os	C	2 H	8 CO	dominant character
$18a_1$ (LUMO)	3.54		1	6	1	92	π^*(CO)
$17a_1$	5.88	8.22	47	7(z)	2	44	$[(Os\text{–}Os)^b, (Os\text{–}CH_2)^b]_{in}{}^c$
$16a_1$	6.49	8.81	31	23(z)		46	$[(Os\text{–}CH_2)^a]_{in}{}^c$
$15b_1$	6.55	8.99	20	52(x)		28	$[(Os\text{–}CH_2)^b]_{in}{}^c$
$14b_1$	7.79	10.19	73	5(x)		22	$[\pi(Os\text{–}Os)^a]_{in}{}^c$
$10b_2$	7.90	10.34	48	15(y)	16	21	$[\delta(Os\text{–}Os)^b, (Os\text{–}CH_2)^b]_{out}{}^c$
$9a_2$	7.97	10.39	72			28	$[\pi(Os\text{–}Os)^a]_{out}{}^c$
$8a_2$	8.46	10.86	69			31	$[\delta(Os\text{–}Os)^a]_{out}{}^c$
$9b_2$	8.78	11.15	67	1(y)	1	31	$[\pi(Os\text{–}Os)^b]_{out}{}^c$
$15a_1$	9.54	12.04	49	35(z)	3	13	$[\pi(Os\text{–}Os)_b, (Os\text{–}CH_2)^b]_{in}{}^c$
$8b_2$	9.97	12.62	16	39(y)	17	28	σ(C–H), $[(Os\text{–}CH_2)^b]_{out}{}^c$
$7a_2$	10.85	13.30				100	σ(CO)

[a] Antibonding. [b] Bonding. [c] Out = out of the Os–CH_2–Os plane (XZ); in = in the Os–CH_2–Os plane (XZ).

Table II. DV-Xα Theoretical Results of $Os_2(CO)_8(\mu\text{-}C_2H_4)$ (2) (C_{2v})

MO	$-\epsilon$, eV	TSIE, eV	pop. % 2 Os	2 C	4 H	8 CO	dominant character
$19a_1$ (LUMO)	3.59		2	8		90	π^*(CO)
$18a_1$	5.90	8.28	44	5(x,z)	1	50	$[(Os\text{–}Os)^b, (Os\text{–}CH_2)^a]_{in}{}^c$
$16b_1$	5.93	8.32	29	46(z)		25	$[(Os\text{–}CH_2)^b, (C\text{–}C)^a]_{in}{}^c$
$10a_2$	7.68	10.00	42	20(y)	20	18	$[\delta(Os\text{–}Os)^a, (Os\text{–}CH_2)^a]_{out}{}^c$
$15b_1$	7.70	10.07	70			30	$[\pi(Os\text{–}Os)^a]_{in}$
$17a_1$	7.83	10.08	46	27(z)		27	$[\pi(Os\text{–}Os)^b, (Os\text{–}CH_2)^a]_{in}$
$9a_2$	8.12	10.43	62	7(y)	6	25	$[\pi(Os\text{–}Os)^a]_{out}$
$16a_1$	8.18	10.72	24	59(x,z)	4	13	$[\pi(Os\text{–}Os)^b, (Os\text{–}CH_2)^b]_{in}$
$10b_2$	8.37	10.71	63	6(y)	4	27	$[\delta(Os\text{–}Os)^b]_{out}{}^c$
$9b_2$	8.91	11.27	68			32	$[\pi(Os\text{–}Os)^b]_{out}{}^c$
$8a_2$	9.04	11.49	37	26(y)	17	20	σ(C–H), $[(Os\text{–}CH_2)^b]_{out}{}^c$
$15a_1$	9.99	12.68	13	68(x,z)	12	7	σ(C–C), $[(Os\text{–}CH_2)^b]_{in}{}^c$

[a] Antibonding. [b] Bonding. [c] Out = out of the Os-CH_2-CH_2-Os plane (XZ); in = in the Os-CH_2-CH_2-Os plane (XZ).

and out-of-phase combinations of p_z orbitals of each CH_2 group. The degree of mixing with the carbon p_x orbitals depends on the actual departure from planarity of the C_2H_4 moiety. In the limiting case of the planar geometry, these two orbitals correlate with the ethylene π and π^* levels.[21] Moreover, the p_x involvement is higher in the $3a_1$ HOMO (18%) than in the $2b_1$ LUMO (4%). For the following analysis it is important to point out that, when fragment **5** assumes the geometry observed in the puckered Os_2C_2 ring, the $3a_1$ HOMO also contains some carbon p_y character and is strongly destabilized (by ca. 1 eV). In contrast the remaining orbitals suffer only minor perturbations. This result can be traced to an interaction between the $3a_1$ HOMO and the inner σ(CH) bonding orbital which involves mainly the carbon p_y orbitals. Note, also, that the symmetry representation of the outermost σ(CH) MO is different in **4** and **5** ($1b_2$ and $1a_2$, respectively, Figure 2).

From the energy data of the frontier MOs reported in Figure 2, it is clear that **4** is at the same time a better donor and a better acceptor group than **5**. The LUMO of **4** lies lower than the LUMO of **5**, whereas the HOMO of **4** is at higher energy than the corresponding MO of **5**. This preliminary observation suggests a better overall interaction of the metallic fragment with **4** than with **5**.

DV-Xα eigenvalues and percentage population analysis of the outermost occupied MOs and of the LUMO of the final complexes **1** and **2** are reported in Tables I and II. The correlation diagram with the orbitals of the constituent fragments is pictured in Figure 2. The assignment of the dominant character of each MO was obtained from symmetry considerations with the help of the diagram previously discussed and from analysis of the respective

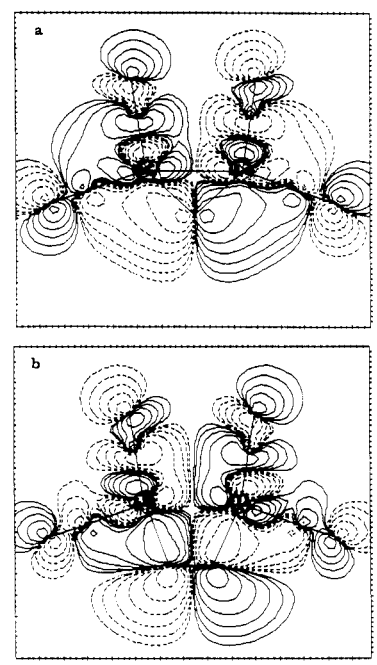

Figure 3. DV-Xα contour plots for (a) $15b_1$ MO of **1** and (b) $16b_1$ MO of **2** in the XZ plane. Contour values are ±0.0032, ±0.0064, ±0.0128, ±0.0256, ±0.0512, ±0.1024, ±0.2048, ±0.4096, ±0.8192 $e^{1/2}/Å^{3/2}$ with negative values in dashed lines.

MO contour plots (CPs). The most interesting contour plots are reported in Figures 3–7.

An important feature during the formation of both compounds **1** and **2** is the emptying of the $16a_1$ HOMO of the metallic fragment **3**. The large interaction between the LUMO of the organic fragment and the LUMO of the inorganic fragment gives rise to an Os–C bonding MO ($15b_1$ in **1** and $16b_1$ in **2**, see Tables I and II and Figures 2 and

(21) It is important to remember that the C–C bond distance in **5** was taken to be equal to the experimental value found in **2**, i.e. 1.53 Å.[5a]

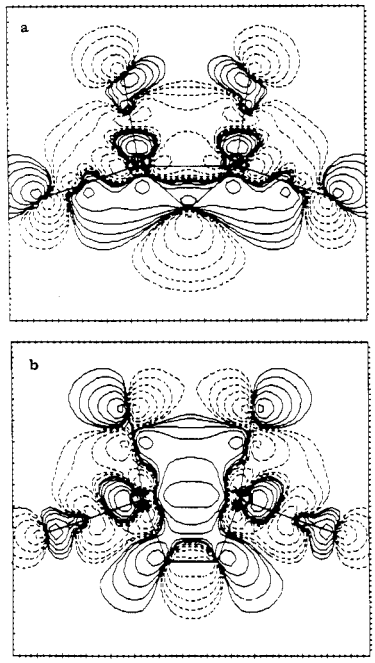

Figure 4. DV-Xα contour plots for (a) $17a_1$ HOMO of **1** and (b) $18a_1$ HOMO of **2** in the XZ plane. Plot parameters are identical with those of Figure 3.

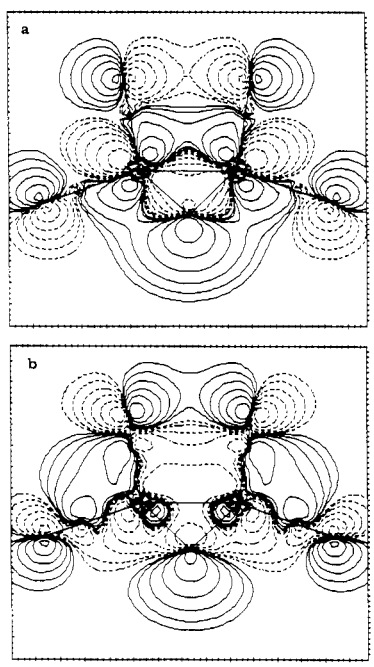

Figure 5. DV-Xα contour plots for (a) $15a_1$ MO and (b) $16a_1$ MO of **1** in the XZ plane. Plot parameters are identical with those of Figure 3.

3) which is more stable than was the $16a_1$ HOMO of **3** and is therefore filled instead of the latter; neither **1** nor **2** contains a filled orbital which corresponds to the $16a_1$ MO of **3**. The net result is that of a charge transfer from the metallic fragment **3** toward the organic substrates. This is clearly seen by the computed negative charges on **4** and **5** in the final complexes (**4**, −0.35 e; **5**, −0.32 e). This fact is in accord with the general conclusion emerging from previous studies of the bonding in polynuclear organometallic molecules of group VIII transition metals, where the importance of the cluster to organic ligand back-donation has been emphasized.[11]

The HOMOs of **1** and **2** ($17a_1$ and $18a_1$, respectively) are both related to the $15a_1$ MO of **3**. They can be described

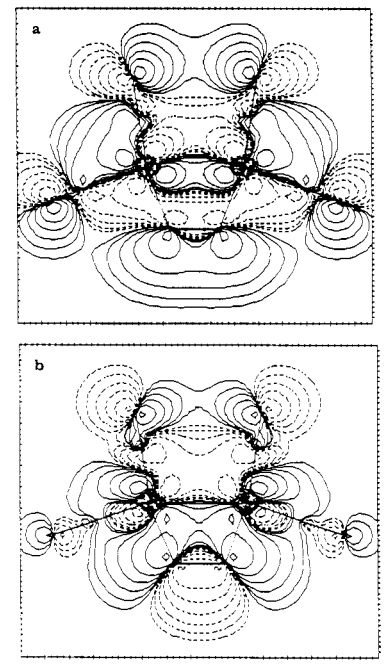

Figure 6. DV-Xα contour plots for (a) $17a_1$ MO and (b) $16a_1$ MO of **2** in the XZ plane. Plot parameters are identical to those of Figure 3.

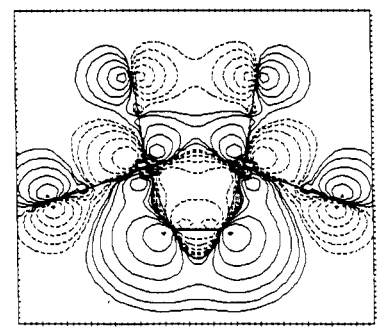

Figure 7. DV-Xα contour plots for $15a_1$ MO of **2** in the XZ plane. Plot parameters are identical with those of Figure 3.

as an Os–Os bonding MO almost completely localized in the XZ plane. These orbitals are responsible for the final Os–Os bond since they have no filled antibonding counterpart. However, some differences between the two HOMOs of **1** and **2** are evident in the CPs reported in Figure 4. The Os–Os interaction is weaker and slightly bent in **1**, the charge bends outwards from the Os–Os edge, whereas it is straight in **2**. This effect follows naturally from the different shapes of the HOMOs of **4** and **5** which interact with the $15a_1$ MO of **3**. In **4**, a carbon p_z lobe points toward the center of the Os–Os bond and bends the metal–metal bond. In **5**, the ethylene n^+ lobes do not perturb the Os–Os bond to a significant extent. Furthermore, the carbon atoms are allowed by symmetry to acquire a p_x contribution in **5** whereas a similar carbon $p_x - p_z$ mixing is not allowed in **4**. As a consequence, a different Os–C interaction in the HOMOs is eventually obtained, bonding in **1** and antibonding in **2**. This fact certainly explains the much lower calculated Os–C overlap population (OP) in **2** (0.22 e) compared to that in **1** (0.39 e). Actually, the partitioning of the overall Os–C OP value into the four a_1, a_2, b_1, and b_2 symmetry contributions clearly demonstrates that the variation is largely due to a reduction in the a_1 component, i.e. in the contribution from the HOMO (**1**, $a_1 = 0.21$, $a_2 = 0.0$, $b_1 = 0.21$, $b_2 = -0.03$e; **2**, $a_1 = 0.08$, $a_2 = -0.01$, $b_1 = 0.18$, $b_2 = -0.03$e). It is interesting to note that, in accord with the calculated

Chart I

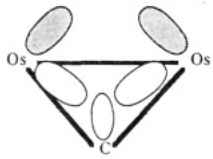

$15a_1$ MO of 1

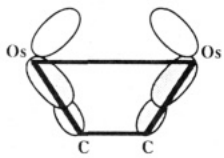

$16a_1$ MO of 2

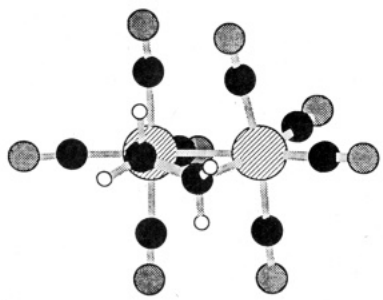

structure of 2

low Os–C overlap population, the extrusion of ethylene and its replacement in **2** by other unsaturated organic substrates are facile processes.[7,9]

The HOMOs of the organic fragments also interact with the t_{2g}-like $14a_1$ MO of **3** of $\pi(Os–Os)_{in}$ character and give rise to the $15a_1/16a_1$ (Table I and Figure 5) and $17a_1/16a_1$ (Table II and Figure 6) partners in **1** and **2**, respectively. However, there are important differences between the two cases. In **1**, there is a large overlap between the carbon p_z orbital and the $14a_1$ MO of **3**, such that a strongly bonding and antibonding pair is formed. The bonding $15a_1$ MO is strongly reminiscent of the Walsh-like bonding MO which accumulates charge inside the triangle of cyclopropane[22] (see the schematic drawing of the $15a_1$ MO of **1** in Chart I). This effect has already been noted in other isolobal analogues of cyclopropane.[4,23] The $16a_1$ MO of **1**, derived from antibonding interaction between the $14a_1$ MO of **3** and the carbon p_z orbital, shows significant contribution from Os 6s,6p orbitals (17%) as a consequence of its interaction with the high-lying $16a_1$ MO of **3**. This interaction stabilizes the $16a_1$ MO, which otherwise would lie at higher energy.

In contrast, a very small energy splitting is computed between the bonding $16a_1$ and antiboding $17a_1$ partners in **2** (0.35 eV in Table II). The better energy match between the $14a_1$ MO of **3** and the $3a_1$ MO of **5** (see Figure 2) is overridden by the weaker Os–C overlaps. It is worthwhile to note the participation of different types of carbon-based orbitals in the $17a_1$ and $16a_1$ MOs, p_z in the former and $p_{x,z}$ in the latter case (Table II and Figure 6). In our opinion this result can be explained by recalling the trapezoidal geometry of the Os_2C_2 ring (see the schematic drawing of the $16a_1$ MO of **2** in Chart I). Thus a significant p_x participation in the $16a_1$ MO (Figure 6b) is needed in order to get a better overlap with the Os orbitals. In contrast to the situation with **1**, this bonding orbital does not accumulate charge into the center of the Os_2C_2 ring and must be related to the b_{1g} MO of the Walsh description of cyclobutane.[24] In the $17a_1$ MO only the p_z contribution is present (see Figure 6a), and, in contrast to **1**, it involves the 6s,6p orbitals of Os only to a very limited extent (1–2%), indicating a very small mixing with the $16a_1$ MO of **3** in this case.

Very interesting is the nature of the innermost $15a_1$ MO of **2**, whose CP is shown in Figure 7. This orbital, strongly reminiscent of the totally symmetric cyclobutane a_{1g} Walsh-like level,[24] represents the only MO which contributes to a charge accumulation inside the Os_2C_2 ring. We must remember, however, that this $15a_1$ MO is mostly localized (68%) on the carbon atoms so that it mainly describes a slightly bent C–C σ bond.

The remaining t_{2g}-like MOs of **3** are perturbed only to a minor extent by the presence of the organic fragments (Figure 2). The only noteworthy interaction occurs between the uppermost σ(CH) bonding orbitals of **4** and **5** ($1b_2$ and $1a_2$, respectively, in Figure 2) with the symmetry-related t_{2g}-like partners of **3**. Accordingly, the $10b_2$ and $10a_2$ MOs of **1** and **2** (see Figure 2 and Tables I and II) have an $(Os–C)_{out}$ antibonding character.

In order to evaluate the bonding modifications induced by the observed puckering of the diosmacyclobutane ring in **2**,[5] we have performed a calculation with the observed solid-state geometry[5] as well (C_2 symmetry, see the schematic drawing of the structure of **2** in Chart I).

The analysis of the bonding scheme is now more complex than in the planar geometry because of the large amount of mixing undergone by the carbon-based orbitals. The n^+(HOMO) and n^-(LUMO) of **5** are now combinations of all three p_x, p_y, and p_z orbitals of each CH_2 group. In addition, as already mentioned, the HOMO of **5** is destabilized when the puckered geometry is assumed, and this is in fact directly responsible for the perturbations computed for the one-electron levels of **2**. In particular, the Os–C OP in the puckered form of **2** decreases slightly (a = 0.06, b = 0.12; total = 0.18e) with respect to the planar geometry (total = 0.22e). This is due to the larger repulsive interaction between the $15a_1$ MO of **3** and the HOMO of the puckered **5**, as a consequence of their better energy matching. Nevertheless, the calculations show that, besides the appearance of an a-type MO approximately 1 eV higher in energy than the $10a_2$ level of the planar Os_2C_2 ring, the energies of the other MOs exhibit little change. Thus it appears that ring puckering does not significantly alter the bonding between the organic and inorganic portions of the molecule. In accord with this is the very high conformational flexibility found in the NMR spectra of the molecule. For this reason, the subsequent analysis of the UV–PE data will be carried out by assuming a planar ring.

NMR Coupling Constants. Bonding schemes are easily tested by the measurement of NMR coupling constants within coordinated ligands. For example, the degree to which the bonding in **1** resembles that in cyclopropane can be evaluated by comparing ^1J(C–H) for these compounds. ^1J(C–H) in **1**, 146.5 Hz, is within the range typical of methylene-bridged dimers.[25] Such values are well above the 125 Hz typical of an acyclic sp^3 carbon but somewhat below that (160 Hz) found for cyclopropane.[26a]

(22) Walsh, A. D. *Trans. Faraday Soc.* **1949**, *45*, 179.
(23) (a) Granozzi, G.; Tondello, E.; Casarin, M.; Ajò, D. *Inorg. Chim. Acta* **1981**, *48*, 73. (b) Calabro, D. C.; Lichtenberger, D. L.; Herrmann, W. A. *J. Am. Chem. Soc.* **1981**, *103*, 6852. (c) Vites, J.; Fehlner, T. P. *J. Electron Spectrosc. Relat. Phenom.* **1981**, *24*, 215.
(24) Hoffmann, R.; Davidson, R. B. *J. Am. Chem. Soc.* **1971**, *93*, 5699.
(25) Herrmann, W. A. *Adv. Organomet. Chem.* **1982**, *20*, 160.
(26) Kalinowski, H.-O.; Berger, S.; Braun, S. *^{13}C-NMR-Spektroskopie*; Georg Thieme Verlag: Stuttgart, 1984; (a) p 446, (b) p 496.

We weould expect a decrease in the $^1J(^{13}C-^{13}C)$ of ethylene upon its coordination of $Os_2(CO)_8$. Such decreases have been observed on coordination of other unsaturated hydrocarbon ligands and have proven useful in testing theoretical analyses of C–C bonding.[27] To test this prediction, we have made **2**-$^{13}C_2$ and measured ^1J(C–C). The result, 34.0 (5) Hz, is almost exactly equal to ^1J(C–C) of ethane (34.6 Hz) and is much less than the value found in ethylene (67.6 Hz),[26b] suggesting that the C–C bond in **2** connects two carbons with sp^3 hybridization. This suggestion supports our conclusion that the $15a_1$ MO is mostly localized on the carbon atoms and mainly describes a C–C σ bond.

UV–PE Data. The lower IE regions (up to 14 eV) of the He I and He II PE spectra of **1** and **2** are shown in Figures 8 and 9, where the bands have been labeled alphabetically. The higher IE spectral region is not considered here because the broad envelope, characteristic of metal carbonyls and due to ionizations from CO based 5σ, 1π, and 4σ orbitals, precludes any productive discussion. The IE values of the region under discussion are reported in Table III together with the proposed assignments.

The theoretical considerations we have presented and literature PE results on related clusters[4a,b,11,23] lead to the expectation of 10 and 11 ionizations for **1** and **2**, respectively, in the spectral region shown in the figures. In both cases, six of these originate from levels derived from the t_{2g}-like set of **3**. The remaining ionizations are from MOs responsible for the bonding within the diosmacycles, including the σ(C–C) MO in **2** and from the uppermost σ-(CH) bonding MO of both organic fragments. In Figures 8 and 9 at least eight and seven different band maxima, with some resolved shoulders are visible for **1** and **2**, respectively. Some of the features show unambiguous relative intensity changes on passing from the He I to the more energetic He II source. For compound **1** (Figure 8) we note an apparent small intensity decrease of the band envelope B–D′, a remarkable intensity falloff for bands G and H, and an increase in the relative intensity of band F. In the spectrum of **2** (Figure 9), band B decreases in intensity, bands C and D appear to decrease a small amount, and band G shows the largest decrease in intensity. Again band envelope F shows an increase in relative intensity. Such relative intensity changes are an important source of information concerning the makeup of the corresponding MOs. Consideration of the Gelius model for the photoionization cross sections[28] (σ), together with the well-documented decreases of the ratios $\sigma(C_{2p})/\sigma(Os_{5d})$ and $\sigma(H_{1s})/\sigma(C_{2p})$ when the more energetic source is used,[11] leads to the conclusion that bands suffering relative intensity decreases are to be associated with ionizations from MOs with important carbon 2p or hydrogen 1s contributions.

The assignments we will propose are mainly based on the following criteria: (i) comparison with the theoretical results discussed before (however, a caveat must be entered here; due to the nonrelativistic nature of the reported calculations and because an estimated geometry was used for **1** in the calculations, no attempts will be made to directly compare the theoretical TSIE values with the experiental ones. Rather, the observed theoretical trends on going from **1** to **2** will be used to rationalize the experimental data); (ii) comparison with PE literature data of related clusters, namely, $Os_3(CO)_{12}$[4] and other dimers containing the μ-(CH_2) bridge;[23] (iii) comparison between the relative band intensities under He I radiation and their changes on switching from He I to the more energetic He II source.

The assignment of band A in **1** and A and B in **2** is straightforward. Band A in both cases is assigned with confidence to the ionizations from the HOMOs $17a_1$ and $18a_1$, respectively, while band B in **2** is associated with the ionization from the $16b_1$ level. Such an assignment is in accord with the decrease in relative intensity, on passing from He I to He II ionization source, of band B of **2** (Figure 9) which has been associated with a MO having a very high percentage (46%) of carbon 2p AOs. The energy of the $16b_1$ MO of **2**, which has a significantly lower IE than the $15b_1$ MO of **1** (vide infra), can be explained on the basis of its very strong π(C–C) antibonding character (see Figure 3).

Before proceeding to the following complex band system, some further considerations must be mentioned. On the basis of the theoretical results, the band system A–E′ most probably contains seven ionizations in **1** and eight in **2**. The extra ionization in **2** is a consequence of the already discussed poor interaction between the $3a_1$ MO of **5** and the suitable t_{2g}-like level of **3**, which results in bonding and antibonding partners $16a_1$–$17a_1$ very close in energy (see Figure 2). In contrast, the strong interaction between the $2a_1$ MO of **4** and the suitable t_{2g}-like level of **3** give rise to a highly destabilized level ($16a_1$ MO of **1**), lying between the eg-like and t_{2g}-like sets, and a highly stabilized level (15a, MO of **1**), the ionization of which is band G in Figure 8. Consequently, it seems reasonable to assign both unresolved band systems, B–E′ of **1** and C–E′ of **2** as a whole, to six ionization events (see Tables I and II, respectively). A more detailed assignment would be hazardous.

The assignment of band F in both cases is more secure. On passing from the He I to He II radiation these bands exhibit substantial increases in relative intensity. In **1**, this band is probably associated with a single ionization originating from the $9b_2$ MO, an orbital with large participation from metal d orbitals. In **2** band F and its shoulder F′ are assigned to the $9b_2$ and $8a_2$ MOs, respectively. The decrease in intensity of the latter under He II radiation is in agreement with the substantial contribution (43%) the organic fragment makes to this MO.

Finally band H in **1** and G in **2** are both related to single ionizations ($8b_2$ in **1**; $15a_1$ in **2**) from levels almost completely localized on the organic portion of the molecules.

Conclusions

Having given a detailed description of the bonding in $Os_2(CO)_8(\mu\text{-}CH_2)$ (**1**) and $Os_2(CO)_8(\mu\text{-}C_2H_4)$ (**2**), which are isolobal to cyclopropane and cyclobutane, respectively, we now wish to compare the bonding schemes of the organic and organometallic analogues.

In cyclopropane there are three MOs, a_1' and e′ under D_{3h} symmetry, that are mostly responsible for the C–C bonding. Adopting the Walsh description,[22] the a_1' orbital accumulates electronic charge at the center of the ring, whereas the e′ MOs distribute electron density around the periphery of the ring. The e′ MOs account, then, for the bent nature of the C–C bonds, which was experimentally verified in a diffraction experiment on a substituted cyclopropane,[29] and determine the chemical properties of this

(27) (a) Benn, R.; Rufinska, A. *J. Organomet. Chem.* **1982**, *238*, C27. (b) Aime, S.; Osella, D.; Giamello, E.; Granozzi, G. *J. Organomet. Chem.* **1984**, *262*, C1 and references therein.

(28) (a) Gelius, U. In *Electron Spectroscopy*; Shirley, D. A., Ed.; North-Holland: Amsterdam, 1972; pp 311–334. (b) Schweig, A.; Thiel, W. *J. Electron Spectrosc. Relat. Phenom.* **1974**, *3*, 27; *J. Chem. Phys.* **1974**, *60*, 951.

(29) Hartman, A.; Hirschfeld, F. L. *Acta Crystallogr.* **1966**, *20*, 80.

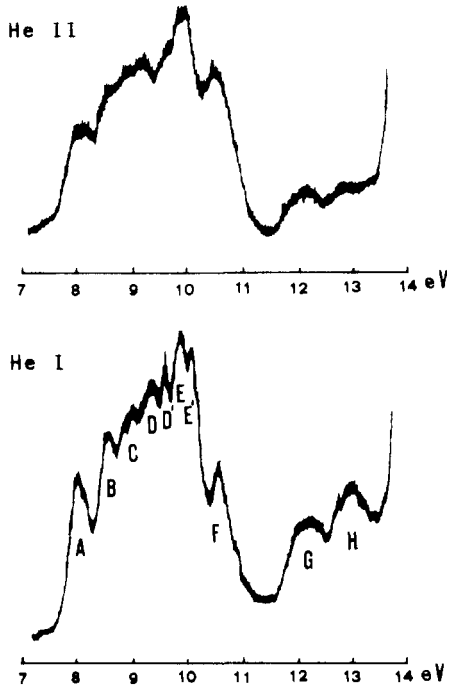

Figure 8. He I (bottom) and He II (top) excited PE spectra of $Os_2(CO)_8(\mu\text{-}CH_2)$ (1).

Table III. UV-PE Data of $Os_2(CO)_8(\mu\text{-}CH_2)$ (1) and $Os_2(CO)_8(\mu\text{-}C_2H_4)$ (2)

$Os_2(CO)_8(\mu\text{-}CH_2)$			$Os_2(CO)_8(\mu\text{-}C_2H_4)$		
band	IE,[a] eV	assign[b]	band	IE,[a] eV	assign[c]
A	8.07	$17a_1$	A	8.00	$18a_1$
B	8.57		B	8.48	$16b_1$
C	9.0		C	9.0	
D	9.3	$16a_1$, $15b_1$, $14b_1$,	D	9.3	$15b_1$, $10a_2$, $17a_1$,
D′	9.6	$10b_2$, $9a_2$, $8a_2$	E	9.67	$9a_2$, $16a_1$, $10b_2$
E	9.87		E′	9.9	
E′	10.03		F	10.46	$9b_2$
F	10.50	$9b_2$	F′	10.7	$8a_2$
G	12.1	$15a_1$	G	11.7	$15a_1$
H	12.9	$8b_2$			

[a] IEs reported are the mean values over several distinct runs. The estimated error is ±0.05 or ±0.1 eV according to the number of decimal places reported. [b] See Table I. [c] See Table II.

molecule. The reported electron-density difference maps of cyclopropane show that the outward shifting of electronic charge from the e′ orbitals is larger than the inward accumulation from the a_1' MO and gives rise to a density depletion at the center of the triangle.[30]

In the organometallic analogue 1, the a_1' and e′ orbitals find a counterpart in the $15a_1$ and $15b_1/17a_1$ MOs, respectively. Their contour diagrams are very similar to those reported for the organic partner.[24] The analogy, however, stops here since an additional orbital ($16a_1$, Table I and Figure 5b) contributes significantly to the framework interactions of the dimetallacyclic ring. The $16a_1$ MO has a large Os–C antibonding character with significant participation from Os 6s,6p orbitals. The reason for the different number of framework orbitals in 1 with respect to cyclopropane is the strong involvement of the t_{2g}-like MOs of the metallic fragments, which do not behave as simple spectators. In particular, the $14a_1$ MO [$\pi(Os\text{–}Os)_{in}$] of $Os_2(CO)_8$ interacts strongly with the HOMO of the CH_2 fragment, giving rise to the aforementioned $16a_1$ level. The

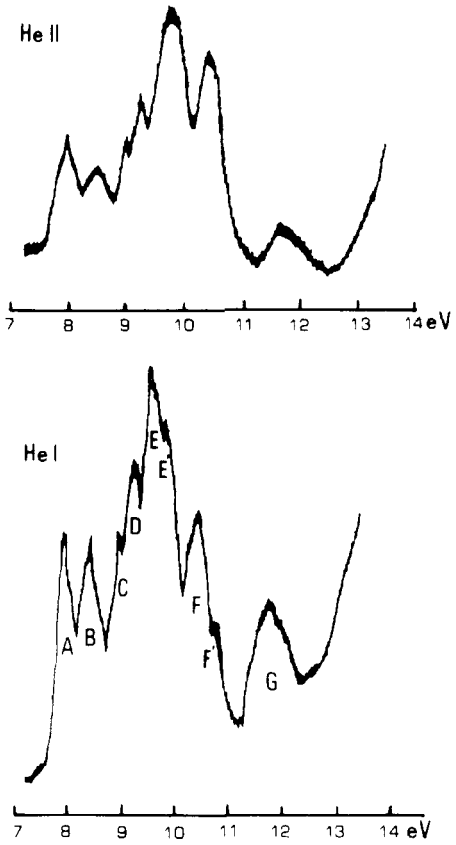

Figure 9. He I (bottom) and He II (top) excited PE spectra of $Os_2(CO)_8(\mu\text{-}C_2H_4)$ (2).

fact that t_{2g}-like orbitals of the $Os(CO)_4$ fragment are not merely a passive electron reservoir has become apparent in other studies of organometallic clusters.[11b,d,e,31]

In a planar (D_{4h}) cyclobutane, the eight electrons involved in the ring bonding occupy, in order to increasing energy, a_{1g}, b_{1g}, and e_u MOs.[24] However a total of five MOs, $15a_1$, $16a_1$, $17a_1$, $16b_1$, and $18a_1$ (see Table II), are now involved in the framework interactions of dimetallacycle 2. The correspondence between the MOs of the two isolobal analogues is as follows: $15a_1$ and $16a_1$ MOs of 2 are related to the a_{1g} and b_{1g} orbitals of cyclobutane, respectively, whereas the quasi-degenerate $18a_1$ and $16b_1$ MOs are the counterparts of the e_u set. As in the three-membered Os_2C ring of 1, an additional orbital, $17a_1$ (Os–C antibonding), originating from the t_{2g}-like set of $Os_2(CO)_8$, is involved in the overall framework interactions of the Os_2C_2 ring of 2.

In conclusion, even though there is ample evidence that the isolobal analogy is "a useful codifier of electronic, structural, and reactivity data, as well as a tool for predicting new compounds and reactions",[32] it is well realized that it is only a model that cannot give full account of all aspects of reality. This is especially true when details of electronic structures and reactivities of isolobal organic and organometallic analogues are compared. The present study provides further evidence that the inner t_{2g}-like orbitals of the metal fragment, normally considered as π-bonding to the M–CO groups only, may also contribute to the metal–ligand interaction especially in multinuclear metal–organic complexes. The challenge for the future is to

(30) Newton, M. D. In *Applications of Electronic Structure Theory*; Schaefer III, H. F., Ed.; Plenum Press: New York; 1977; Chapter 6 and references therein.

(31) (a) Sherwood, D. E., Jr.; Hall, M. B. *Inorg. Chem.* **1982**, *21*, 3458. (b) Chesky, P. T.; Hall, M. B. *Inorg. Chem.* **1983**, *22*, 3327.

(32) Albright, T. A.; Burdett, J. K.; Whangbo, M. H. *Orbital Interactions in Chemistry*; Wiley: 1985; pp 402–403.

assess the extent and the chemical consequences of such interactions.

Acknowledgment. This research was supported by NATO Collaborative Research Grants RG 86/0553 and 83/983, by the US Department of Energy, Grant DE-FG02-84ER13299.A004, and by Natural Sciences and Engineering Research Council of Canada, Grant A6659. We thank Professor Roald Hoffmann for constructive comments and Mr. F. De Zuane for technical assistance.

Registry No. 1, 83705-04-8; 2, 83705-05-9.

Synthesis of [η^5-(Diphenylphosphino)cyclopentadienyl][η^7-(diphenylphosphino)cycloheptatrienyl]titanium and Its Utility in the Formation of Heterobimetallic Complexes: The Molecular Structure of Tetracarbonyl{[η^5-(diphenylphosphino)cyclopentadienyl][η^7-(diphenylphosphino)cycloheptatrienyl]titanium-*P*,*P'*}chromium Hemitoluene Solvate

Lawrence B. Kool,[1] Masao Ogasa,[2] and Marvin D. Rausch*

Department of Chemistry, University of Massachusetts, Amherst, Massachusetts 01003

Robin D. Rogers*

Department of Chemistry, Northern Illinois University, DeKalb, Illinois 60115

Received January 5, 1989

Treatment of (η^5-C_5H_5)(η^7-C_7H_7)Ti with 2.4 equiv of *n*-BuLi/TMEDA followed by reaction with Ph_2PCl has afforded the titanium diphosphine complex (η^5-$C_5H_4PPh_2$)(η^7-$C_7H_6PPh_2$)Ti (**5**) in high yield. Complex **5** reacts with a variety of metal carbonyls in refluxing toluene to produce a series of chelated heterobimetallic compounds, including [(η^5-$C_5H_4PPh_2$)(η^7-$C_7H_6PPh_2$)Ti]$M(CO)_4$ [M = Cr (**6**); Mo (**7**)], [(η^5-$C_5H_4PPh_2$)(η^7-$C_7H_6PPh_2$)Ti](η^5-C_5H_5Co) (**8**), and [(η^5-$C_5H_4PPh_2$)(η^7-$C_7H_6PPh_2$)Ti]$Fe(CO)_3$ (**9**). ^{31}P NMR spectra of both **7** and **9** indicate phosphorus–phosphorus coupling as a result of coordination to the same metal atom. The crystal structure of the hemitoluene solvate of **6** has been carried out. It crystallizes in the triclinic space group $P\bar{1}$ with (at −150 °C) a = 10.478 (6) Å, b = 11.012 (7) Å, c = 17.679 (8) Å, α = 82.05 (5)°, β = 79.39 (5)°, γ = 84.01 (5)°, and D_{calcd} = 1.31 g cm^{-3} for Z = 2. A toluene molecule is disordered about a center of inversion. The phosphino groups are both on the same side and coordinated to the Cr atom (Cr–P(average) = 2.43 (2) Å). The Ti–C(η^7) and Ti–C(η^5) distances average 2.19 (1) and 2.31 (2) Å, respectively, with an observed Cent(C_5)–Ti–Cent(C_7) angle of 173.5°. The parent compound **5** was also crystallographically characterized. **5** is monoclinic, $P2_1/c$, with (at 20 °C) a = 8.611 (3) Å, b = 18.633 (5) Å, c = 9.110 (3) Å, β = 98.02 (3)°, and D_{calcd} = 1.31 g cm^{-3} for Z = 2. The molecule is disordered about a crystallographic center of inversion; the phosphorus atoms thus are trans to one another. Important parameters include Ti–C(η^7) = 2.19 (5) Å (average), Ti–C(η^5) = 2.34 (3) Å (average), and Cent(C_5)–Ti–Cent(C_7) = 175.8°.

Introduction

There is currently considerable interest in the synthesis, properties, and structures of heterobimetallic compounds in which the two metals are held in close proximity by heterodifunctional ligands.[3,4] Studies have focused especially on complexes that contain both early (electron-deficient) and middle or late (electron-rich) transition metals, since such systems might exhibit cooperative reactivity.[3,4] While heterobimetallics with a wide variety of bridging ligands are now known, some of the most readily accessible systems are those derived from metallocene-type units that contain two symmetrically positioned diphenylphosphino substituents. These compounds may be regarded as chelating diphosphines that are linked by an organometallic moiety. Subsequent reactions with metal carbonyls or with transition-metal halides lead directly to heterobimetallic compounds in which the two phosphine units become chelated to the second metal. 1,1′-Bis(diphenylphosphino) derivatives of ferrocene,[5–10] cobaltoc-

(1) Current address: Department of Chemistry, Boston College, Chestnut Hill, MA 02167.

(2) On sabbatical leave from the Corporate Research Institute, Sekisui Chemical Co., Ltd., Osaka, Japan, 1987–1989.

(3) Bullock, R. M.; Casey, C. P. *Acc. Chem. Res.* **1987**, *20*, 167. See also references cited therein.

(4) White, G. R.; Stephan, D. W. *Organometallics* **1988**, *7*, 903. See also references cited therein.

(5) Whitesides, G. M.; Gaasch, J. F.; Stedronsky, E. R. *J. Am. Chem. Soc.* **1972**, *94*, 5258.

0276-7333/89/2308-1785$01.50/0